The influence of mineral particles on fibroblast behaviour: A comparative study

Soto Véliz, Diosangeles; Luoto, Jens; Pulli, Ilari; Toivakka, Martti

Published in:
Colloids and Surfaces B: Biointerfaces

DOI:
10.1016/j.colsurfb.2018.04.013

Published: 01/01/2018

Document Version
Accepted author manuscript

Document License
CC BY-NC-ND

The influence of mineral particles on fibroblast behaviour: a comparative study

Diosangeles Soto Veliz[a,*], Jens C. Luoto[b], Ilari Pulli[b], and Martti Toivakka[a]

[a]Laboratory of Paper Coating and Converting, Center for Functional Materials, Åbo Akademi University, Porthaninkatu 3, 20500 Turku, Finland
[b]Cell Biology, Åbo Akademi University, Tykistökatu 6A, 20520 Turku, Finland
*Corresponding author: diosangeles.sotoveliz@abo.fi

ABSTRACT

Minerals are versatile tools utilised to modify and control the physical-chemical and functional properties of substrates. Those properties include ones directing cell fate; thus, minerals can potentially provide a direct and inexpensive method to manipulate cell behaviour. This paper shows how different minerals influence human dermal fibroblast behaviour depending on their properties. Different calcium carbonates, calcium sulphates, silica, silicates, and titanium dioxide were characterised using TEM, ATR-FTIR, and zeta potential measurements. Mineral-cell interactions were analysed through MTT assay, LDH assay, calcein AM staining, live cell imaging, immunofluorescence staining, western blot, and extra/intracellular calcium measurements. Results show that the interaction of the fibroblasts with the minerals was governed by a shared period of adaptation, followed by increased proliferation, growth inhibition, or increased toxicity. Properties such as size, ion release and chemical composition had a direct influence on the cells leading to cell agglomeration, morphological changes, and the possible formation of protein-mineral complexes. In addition, zeta potential and FTIR measurements of the minerals showed adsorption of the cell culture media onto the particles. This article provides fundamental insight into the mineral-fibroblast interactions, and makes it possible to arrange the minerals according to the time-dependent cellular response.

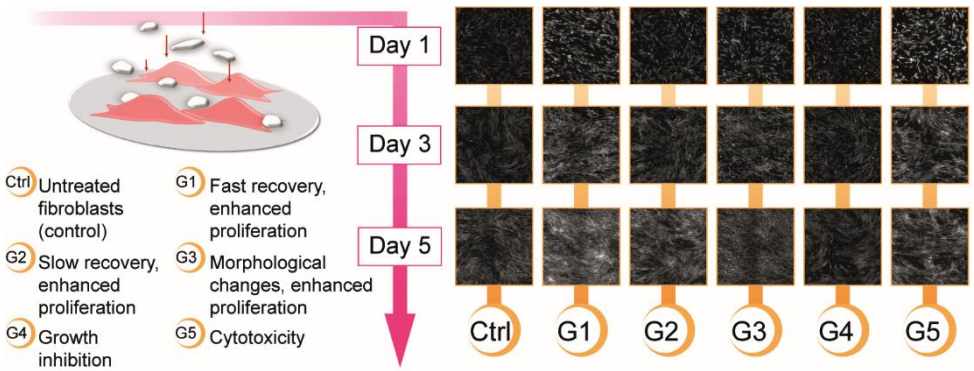

Keywords: Mineral, particle, fibroblast, behavior, biocompatibility

INTRODUCTION

Cell fate depends strongly on the physical-chemical properties of the extracellular environment. Cells are able to sense cues from their vicinity and respond with processes such as protein expression, cell differentiation, migration, proliferation, and death [1-3]. Therefore, it is possible to control cell decision-making through the modification of the extracellular features. Current standard methods for cell culture do not facilitate such modifications nor mimic native extracellular environment. Thus, the development of a cell-instructive platform would allow further understanding of the mechanisms underlying cellular processes, and potentially reduce the gap between *in vitro* and *in vivo* studies.

Minerals are utilised to modify and improve physical-chemical properties of substrates, including those relevant for the cell machinery, such as surface energy, roughness or porosity. In a race to develop smart environments for cell growth, minerals can provide the means to control and regulate cell behaviour. As particles, minerals can be used as additives in matrices, as fillers, surface coatings or porous packed structures [4]. The versatility of minerals lies in the easiness to manipulate the resulting properties of a system through changes to particle size, shape, hydrophobicity, and surface structure. Size, in particular, is relevant for cell behaviour since nanoparticles can be internalised by cells and potentially exert a toxic response. It is also possible to functionalise mineral surfaces through the adsorption of molecules.

Traditionally, the largest use of minerals, such as calcium carbonates, calcium sulphates, silica, silicates, and titanium dioxide, is in the paper industry, as fillers and in paper coatings [5]. Nowadays, the biological applications of minerals is rapidly expanding. The osteogenic potential of calcium-based minerals is an advantage in bone engineering where they are used as fillers, coatings, implants or scaffolds [6-10]. As part in composites, calcium carbonate provides improved stability for long term use. In contrast, calcium sulphates have a fast resorption rate that, together with its pH-dependent solubility [11], increases locally the concentration of calcium, which is a crucial ion in cell signalling [12]. Additionally, both calcium-based minerals support the encapsulation of biomacromolecules and induce a controlled drug or gene delivery [13-15]. Silica is used in the delivery of biomolecules, cell labelling, cell growth coatings, bone engineering, cancer treatment and in drug tracking studies [16-20]. Natural silica (diatomite) has excellent capabilities for drug delivery and particle functionalisation due to their highly ordered multiporous structures [21,22]. Silicates such as kaolin and zeolite induce the haemostatic response in the body. They are used as clotting agents in commercial wound healing dressings to stop haemorrhagic bleeding [23]. Until recently, biocompatibility studies related to kaolin showed increased toxicity [24-26], yet nowadays kaolin is a promising material for novel drug delivery systems [27,28]. In contrast, literature regarding the influence of talc on cells is limited and/or outdated [29-34] regardless of its unique properties such as high thermal stability, low conductivity, high oil absorptivity, high aerophilicity and hydrophobicity [35,36]. Lastly, the photocatalytic properties of titanium dioxide is applied in photodynamic cancer treatments, coating of implants, drug delivery, cell labelling, biosensing, and genetic modification of cells [37].

Despite the research available on minerals in a biological environment, there are no guidelines to predict how specific cell lines will respond to new samples. Hence, the principles behind the influence of mineral properties on cell behaviour remain to be explored. This article assesses and compares the effect of selected minerals and their properties on cell behaviour. The screening of the minerals helps to elucidate possible future applications in cell-instructive platforms such as the paper-based cell growth platform [38-40].

MATERIALS AND METHODS

Table 1 shows the label, commercial name, material supplier, and general description of the minerals selected for this research. The selected minerals were: calcium carbonates of various sizes, calcium sulphates with different hydrated states, silica of both natural and synthetic origin, several silicates, and titanium dioxide. Commercial grades of minerals often contain additives such as dispersing agents to improve their dispersability in aqueous systems [4]. These additives may affect the cellular response, adding some degree of uncertainty to the study.

Table 1. Description and source of the mineral particles utilised in this research.

Label	Commercial name	Supplier	Additional information
CCCARB	Carbital™ 140	Imerys Minerals Ltd, UK	Large ground calcium carbonate ($CaCO_3$)
CCOBIND	Optibind PCC	Imerys Minerals Ltd, UK	Precipitated calcium carbonate ($CaCO_3$)
CCHC90	Hydrocarb® 90	Omya International AG, CH	Ultrafine ground calcium carbonate ($CaCO_3$)
CCOMYA	-	Omya International AG, CH	Experimental grade carbonate-based specialty pigment
CS2H2O	Calcium sulfate dihydrate, ReagentPlus® (C3771-500G)	Sigma-Aldrich Co., USA	Calcium sulphate dihydrate, ≥ 99% ($CaSO_4.2H_2O$)
CSANAL	-	Sigma-Aldrich Co., USA	Calcium sulphate dihydrate ($CaSO_4.2H_2O$) analytical standard
CSINDUS	-	Sigma-Aldrich Co., USA	Calcium sulphate hemihydrate ($CaSO_4.0.5H_2O$) industrial standard
CS325M	Calcium sulfate (237132-500G)	Sigma-Aldrich Co., USA	Anhydrous calcium sulphate ($CaSO_4$) ~325 Mesh, 99%
SYC807	Syloid C807	W. R. Grace & Co.-Conn., USA	Amorphous synthetic silica
DECE209	Celite® 209	Imerys Minerals Ltd, UK	Diatomite
DEDF525	Diafil® 525	Imerys Minerals Ltd, UK	Diatomite
SYSM405	Sylowhite™ SM405	W. R. Grace & Co.-Conn., USA	Precipitated amorphous sodium aluminium magnesium silicate
ZEIMER	-	Imerys Minerals Ltd, UK	Experimental grade zeolite (aluminosilicate mineral)
TAC15	Finntalc C15	Mondo Minerals B.V., NE	Finnish talc (hydrated magnesium silicate) including 0-4% of chlorite, dolomite and magnesite
KAINT57	Intramax 57	Imerys Minerals Ltd, UK	Kaolin (hydrated aluminium silicate) lump china clay
KABSHX	Barrisurf™ HX	Imerys Minerals Ltd, UK	Hyper-platy kaolin (hydrated aluminium silicate) (shape factor 100)
KABSLX	Barrisurf™ LX	Imerys Minerals Ltd, UK	Hyper-platy kaolin (hydrated aluminium silicate) (shape factor 60)
TDKEM	Titanium dioxide	Kemira Oyj, FI	Titanium dioxide (TiO_2) RDE2

Mineral particle characterisation

Particle size and morphology were studied using Transmitted Electron Microscopy (JEM-1400 Plus TEM, Jeol Ltd.). Minerals were classified with different geometrical features of their morphology, and parameters characterising the particles were collected through image analysis (protocol in Appendix A). Minerals were also immersed in cell culture media (with and without serum) for one and three days, then washed with deionised water, centrifuged at 2000×g and dried before further characterisation. Attenuated total reflectance infrared spectroscopy (ATR-FTIR, Thermo Scientific Nicolet iS50 Spectrometer) and zeta potential measurements (Zetasizer 3000, Malvern Instruments Ltd.) were conducted on the minerals before and after immersion.

Cell culture

The Human Dermal Fibroblast (HDF, human, neonatal, ATCC® PCS-201-010™) cell line was provided by Prof. John Eriksson at Åbo Akademi University. This cell line was selected due to its role in dermo-epidermal interactions; and consequently, its relevance for dermal tissue engineering [41], an area of application for instructive platforms. The HDFs were cultivated with Dulbecco's Modified Eagle's Medium (DMEM, Sigma-Aldrich) supplemented with 10% Foetal Bovine Serum (FBS, Biowest), penicillin-streptomycin (10000 units/10mg per mL, Sigma-Aldrich), and L-glutamine (200 mM, Biowest). Cells were incubated at 37 ºC with an atmosphere containing 5% CO_2 and 95% relative humidity.

Treatment of cells with the mineral particles

HDFs were treated with the different minerals to assess their interaction. Both cell, and mineral seeding had an equivalent cell/cm^2 and mineral/cm^2 ratio throughout different sized multi-well plates (Appendix Table A.1). Cells were grown until 80-90% confluency, and subcultured as needed. The following day, minerals were dispersed in serum-free DMEM by 20 minutes ultrasonication and vortexing. The stock dispersions were diluted to the calculated initial concentration and the minerals were seeded to the wells whereby the concentration was halved (final concentration). HDFs were exposed to the minerals for up to five days, and tested at different time points as required by the various assays. Cells grown in cell culture media (50% complete, 50% serum-free) without mineral particles were used as positive control, and cell culture media without cells, but with minerals, served as negative control. In the biological assessment, at least three different biological replicates were utilised throughout the study.

Cell imaging and microscopy

Live cell imaging in 96-well plates was conducted with the Cell-IQ® imaging system for a period of five days. Additional plates were stained with 5 µM Calcein AM (ThermoFisher Scientific) at day one, three, and five of the treatment, and consequently imaged. To investigate cell morphology, HDFs were stained for cell nuclei, actin cytoskeleton, and vimentin filaments after three days of treatment (protocol in Appendix A). Images were obtained using a 3i spinning disk confocal microscope (Cell Imaging Core, Turku Centre for Biotechnology, Finland).

Cytotoxicity assessment

MTT (Sigma-Aldrich) and LDH (ThermoFisher Scientific) assays were used to study the metabolic activity/viability of cells and cell damage/cytotoxicity, respectively (Protocols in Appendix A). The assays were performed in 96-well plates at one, three, and five days of treatment.

Western blotting: Stress, and apoptotic markers

After three days of treatment, HDFs were harvested from 6-well plates by washing with PBS, followed by scraping in lysis buffer and placed in microcentrifuge tubes. The lysates were incubated on ice for 30 minutes, followed by centrifugation at 20,000×g for 10 minutes at 4 °C. The supernatants (cell lysates) were used for western blot analyses. The cell lysates' protein concentrations were determined by Bradford assay and equal sample protein amounts were separated by SDS-PAGE. Proteins were transferred to nitrocellulose membranes, and upon immunoblotting, visualized by enhanced chemiluminescence. Immunoblotting was performed with antibodies against HSF1 (rabbit, SPA-901, 1:4000; Enzo Life Sciences), Hsp27 (mouse, SPA-803, 1:4000; Enzo Life Sciences), Hsp70 (mouse, SPA-810, 1:5000; Enzo Life Sciences), Hsp90 (rabbit, SPA-830 1:4000; Enzo Life Sciences), and PARP1 (mouse IgG2a, (F-2): sc-8007, 1:1000; Santa Cruz Biotechnology). Alpha tubulin (mouse, 12G10, 1:1000; Developmental Studies Hybridoma Bank) was used as a loading control.

Calcium ion release assessment

Cells were treated in 96-well plates with calcium releasing minerals (CS2H2O, CSANAL, CSINDUS, and CS325M) for one day in calcium-free, serum-free or 50:50 serum-free/complete DMEM. Before treatment, all cell culture media was removed from the wells, washed with PBS, and substituted with the required cell culture media. The Calcium Colorimetric Assay (Sigma-Aldrich) was used to measure the calcium ion concentration as stated in its protocol.

Intracellular calcium measurements using the ratiometric fluorescent calcium indicator Fura-2AM

HDFs were treated in 96-well plates with the calcium releasing minerals (CS2H2O, CSANAL, CSINDUS, and CS325M) for one day. Thereafter, the cells were washed three times with HEPES-buffered saline solution (HBSS) and incubated with 2 μM Fura-2AM (Life Technologies) for 30 minutes at room temperature. Then, the cells were washed twice and incubated in HBSS for 15 minutes, followed by two washes. The calcium measurements (excitation at 340 and 380 nm, and emission at 510 nm) were conducted in a Hidex Sense plate reader equipped with a dispenser unit to deliver the agonist histamine (Sigma-Aldrich) to the cells. The ratio of the calcium unbound and calcium bound Fura-2 excitations (F_{340}/F_{380}) was calculated for each timepoint of the measurements, and the obtained values were used for analysis of the data.

Image processing

Image processing package Fiji ImageJ [42,43] was used to process, analyse, and quantify all the data collected through microscopy, and from the western blotting.

Statistics

The software GraphPad Prism 7 was used for the statistical analysis of the Western blotting results. The treated cells were compared to untreated cells and between each other using ANOVA, followed by Tukey's test.

RESULTS AND DISCUSSION

In this section, first the mineral particles are characterised according to their morphology. Then, the effect of the cell culture media on the minerals is assessed, followed by discussion of the role of the mineral properties on the cellular response of fibroblasts.

Mineral particle characterisation

Figure 1 contains representative images of the mineral particles studied and Table 2 shows the corresponding descriptions obtained from the image analysis of the TEM data. Parameters selected to characterise the morphology of the particles were the general shape, the equivalent circular diameter at the cumulative area 10%, 50%, and 90%, and the aspect ratio. In the mineral SYC807, there are two different sizes to consider. The size in the table refers to the size of the aggregates, while the individual particles, visible at higher magnifications, are below 20 nm. Minerals CCCARB, CS325M, TAC15, and KAINT57 had the broadest particle size distributions while the minerals CCOBIND, CCHC90, SYSM405, and TDKEMIR had the narrowest ones when compared to the rest of the samples.

Image analysis was not suitable for the measurement of DECE209 and DEDF525. The morphological features of the two diatomites were difficult to quantify since the minerals broke down into highly irregular pieces. From the images, it is visible that DECE209 contains mostly frustules of centric diatoms while DEDF525 contains mostly pennate diatoms. Both minerals have a particle size up to 30 μm with pores ranging 100-500 nm in size in the hierarchical structure of the frustule.

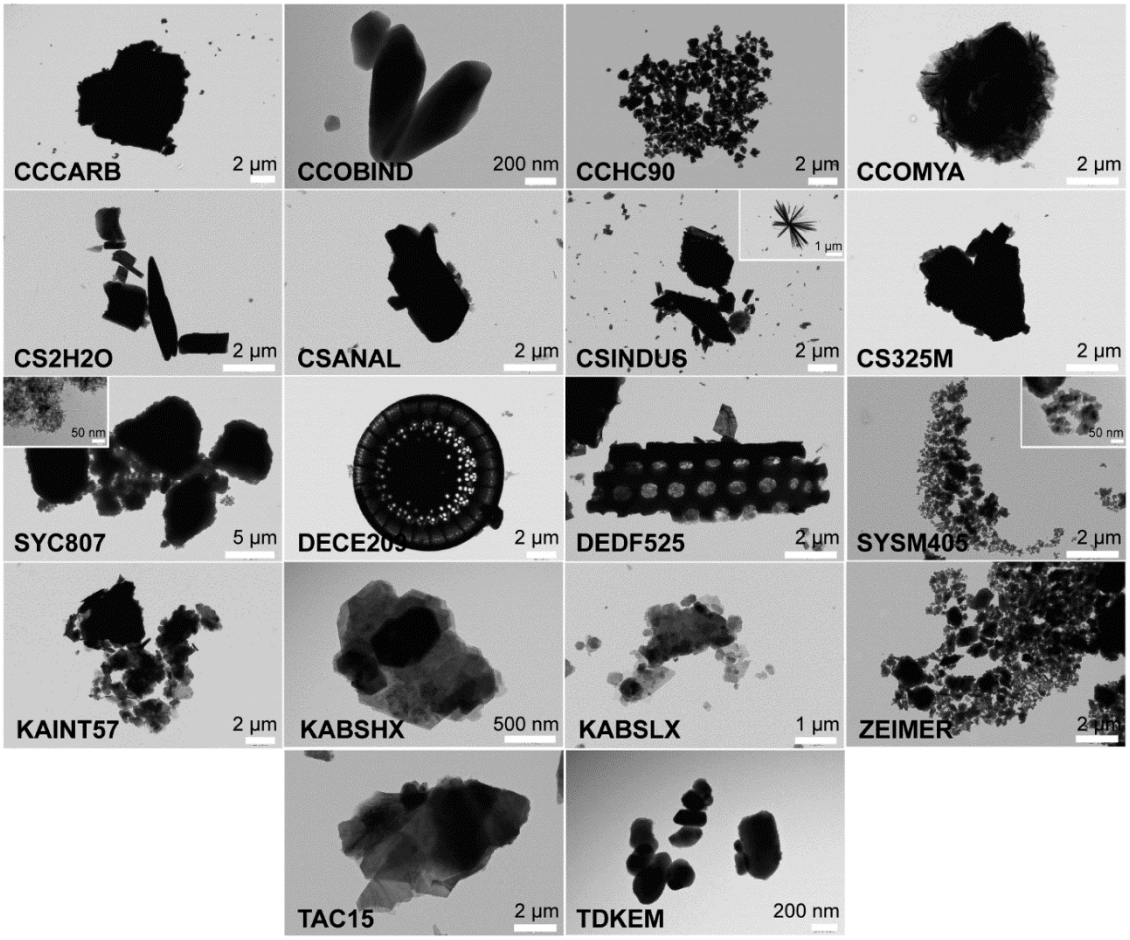

Figure 1. Representative TEM images of the mineral particles.

Table 2. Mineral particle shape, size, aspect ratio (AR) and specific surface area (SSA). Size is expressed as equivalent circular diameter in µm of cumulative 10% (D10), 50% (D50), and 90% (D90). The specific surface area in m^2/g was obtained from the manufacturers.

Mineral	Shape [-]	D10 [µm]	D50 [µm]	D90 [µm]	AR [-]	SSA [m^2/g]
CCCARB	Angular	0.73	4.84	12.26	1.58	2
CCOBIND	Cylindrical/ellipse	0.40	0.81	2.58	1.76	9
CCHC90	Angular	0.35	0.88	1.84	1.49	12.5
CCOMYA	Irregular	1.09	5.21	8.42	1.56	53
CS2H2O	Angular	0.60	2.64	7.56	1.75	-
CSANAL	Platy + Angular	0.32	1.72	7.43	1.78	-
CSINDUS	Acicular + angular	0.35	1.24	8.73	1.77	-
CS325M	Angular	0.88	5.01	13.99	1.64	-
SYC807	Round/angular	1.61	5.42	10.25	1.53	-
DECE209	Irregular porous	-	-	-	-	25
DEDF525	Irregular porous	-	-	-	-	30
SYSM405	Platy	0.11	0.52	1.70	1.53	-
ZEIMER	Platy/Angular	0.52	2.66	6.93	1.55	-
TAC15	Platy	1.70	6.26	12.55	1.67	6
KAINT57	Platy	1.22	5.28	12.19	1.55	10
KABSHX	Platy	0.45	1.51	4.74	1.56	11-12
KABSLX	Platy	0.57	2.15	8.31	1.55	17
TDKEMIR	Round/angular	0.23	0.36	0.59	1.46	-

Table 2 also shows the specific surface area of the minerals, when available from the manufacturer. In this study, no correlation was observed between the specific surface area and the resulting behaviour in the cells. However, specific surface area and porosity are important parameters that must be studied in more detail in the future to fully understand the surface-induced conformational changes during protein adsorption to the minerals.

Influence of the cell culture media on the mineral particles

FTIR spectra were used to study changes to the mineral particle surfaces after immersion in cell culture media. The spectra were acquired before and after autoclaving, followed by one and three days of immersion in serum-free and complete DMEM. Figure 2 shows the range of wavelengths where changes were observed. The full range of wavelengths and descriptions are in Appendix Figure A.1-18.

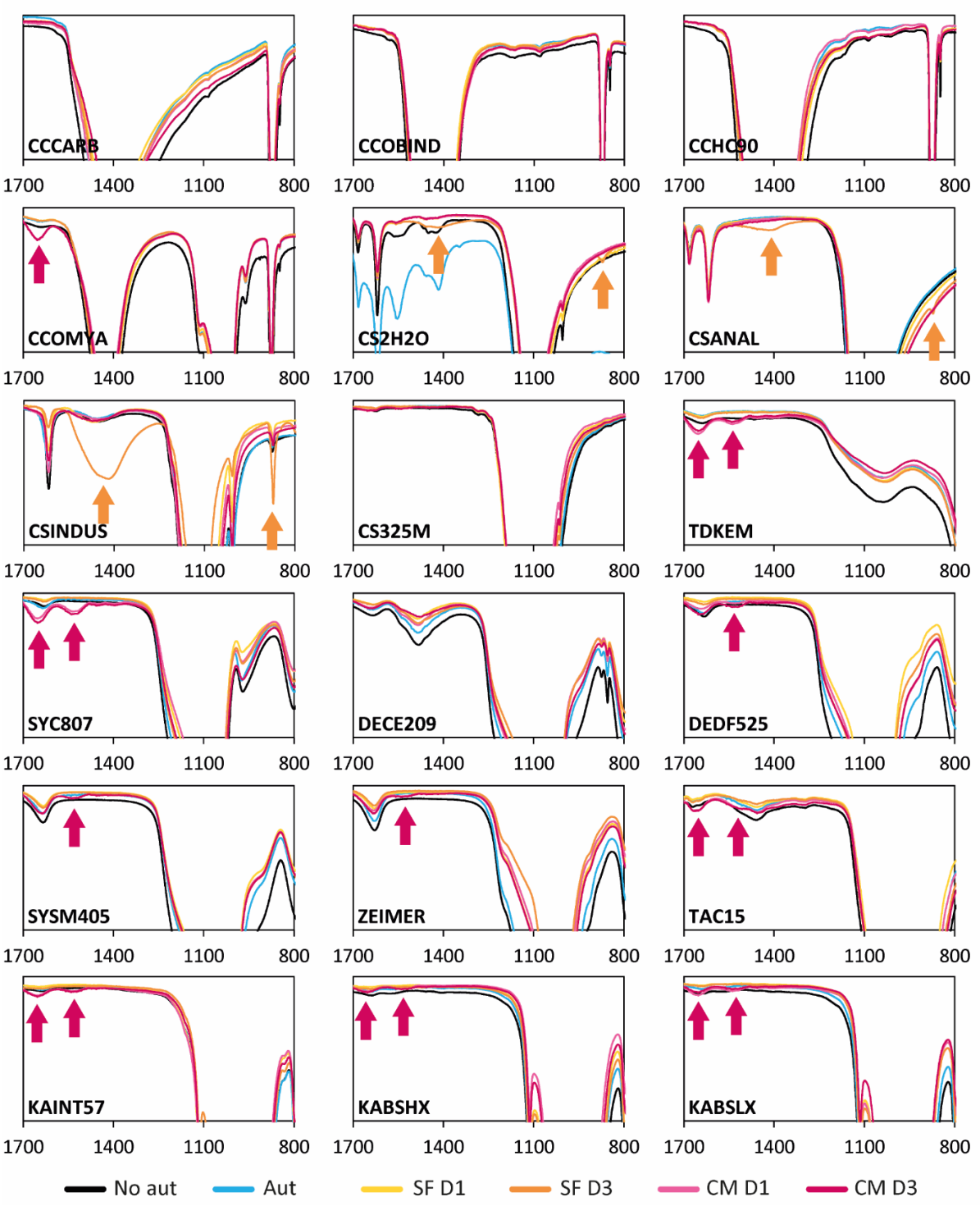

Figure 2. FTIR spectra for the minerals before (No Aut) and after (Aut) autoclaving, and after one (D1) and three (D3) days of immersion in serum-free DMEM (SF), and in complete DMEM (CM). Orange and magenta arrows indicate the changes after immersion in the serum-free and complete DMEM, respectively.

Minerals CCOMYA, TDKEM, SYC807, SYSM405, ZEIMER, TAC15, KAINT57, KABSHX, and KABSLX exhibit new peaks in the regions 1510-1540 and 1630-1670 cm^{-1} after immersion in complete DMEM. Since the change occurred only in complete DMEM, it is attributed to serum which has protein bovine serum albumin (BSA) as its major component [44]. The placement of the new peaks is comparable to those for BSA [45,46] and shared by other proteins. The peaks around 1630-1670 cm^{-1}

represent the amide I band of proteins, and the peaks in 1510-1540 cm^{-1} are representative for the amide II band [47]. Therefore, there is adsorption of the serum proteins onto the minerals surface. The shift between the peaks in the different minerals represents changes in structural form of the protein arrangement (α-helix, β-helix, and random coil). The quantity and method of adsorption depend on the preferential binding sites available in each mineral and will determine the final structural conformation of the proteins [48]. Surface-induced conformational changes to proteins are important for material-cell interactions since many cellular processes depend on the surface protein layer [49].

Calcium sulphates with a hydrated state (CS2H2O, CSANAL, and CSINDUS) presented new peaks only after three days of immersion in serum-free DMEM at the wavelengths of 1410-1420 and 800-890 cm^{-1}. These changes suggest that the interaction occurs with a component of the serum-free cell culture media and that such interaction is inhibited in the presence of serum. The hemihydrated sample (CSINDUS) has the highest peaks in both regions, possibly due to higher availability of active sites. In contrast, unmodified calcium carbonate (CCCARB, CCOBIND, CCHC90), calcium sulphate anhydrate (CS325M), and diatomite (DECE209) did not experience any significant changes to their spectra regardless of the cell culture media, suggesting no adsorption of molecules onto the mineral surfaces. However, the diatomites had peaks in the region of interest in the original sample which can be attributed to organic impurities attached to the frustules.

To further understand the influence of the cell culture media on the minerals, zeta potential was measured before and after autoclaving and after one and three day immersion in serum-free and complete cell culture media (Table 3). The pH of the cell culture media during the mineral-cell interaction was between 7.2-7.6 throughout the experiments.

Table 3. Zeta potential of mineral particles, and the standard deviation of the measurements (Δ), before and after sample preparation, and after one and three day immersion in serum-free and complete cell culture media.

Minerals	Non autoclaved		Autoclaved		Serum-free Day 1		Serum-free Day 3		Complete Day 1		Complete Day 3	
	mV	Δ	mV	Δ	mV	Δ	mV	Δ	mV	Δ	mV	Δ
CCCARB	-5.2	0.7	-11.2	4.0	-13.5	0.8	-15.0	0.6	-17.0	0.5	-20.3	0.5
CCOBIND	22.4	0.8	14.8	0.3	-1.2	0.2	-0.9	0.3	-21.0	0.7	-21.3	0.4
CCHC90	-21.5	0.6	-22.3	0.6	-23.6	0.8	-24.8	0.6	-20.5	0.6	-19.9	0.5
CCOMYA	14.3	0.1	16.3	0.2	16.0	0.4	15.8	0.5	-18.2	0.2	-19.3	0.3
CS2H2O	-3.0	0.4	-3.1	1.7	-2.6	0.7	-2.2	0.3	-3.1	1.4	-6.9	2.3
CSANAL	-6.1	2.5	-3.3	0.9	-4.8	1.5	-2.3	0.2	-12.3	3.2	-3.9	1.5
CSINDUS	-15.7	0.5	-9.8	2.5	-7.0	1.0	-2.7	0.7	-19.6	0.9	-17.3	0.3
CS325M	-5.7	1.9	-2.7	0.4	-4.2	0.3	-3.7	1.5	-17.9	0.3	-18.1	0.3
SYC807	-14.3	1.0	-13.7	1.1	-8.5	0.7	-16.9	0.3	-11.2	0.4	-17.5	0.6
DECE209	-21.6	0.5	-17.9	0.3	-18.1	0.8	-19.1	0.3	-16.1	0.6	-19.5	0.4
DEDF525	-20.1	0.4	-13.7	1.4	-26.8	1.9	-25.4	0.7	-21.9	0.4	-22.2	0.2
SYSM405	-32.5	1.0	-30.9	0.6	-28.6	1.0	-27.6	0.7	-23.5	0.3	-23.7	0.2
ZEIMER	-27.6	1.7	-23.3	1.2	-28.6	0.9	-25.5	1.0	-23.9	0.7	-25.5	0.3
TAC15	-22.7	1.0	-11.9	2.6	-20.0	0.9	-19.9	1.5	-20.4	1.8	-21.5	1.7
KAINT57	-23.1	0.7	-14.9	2.5	-16.9	1.6	-20.6	0.4	-16.5	1.4	-20.2	1.4
KABSHX	-34.0	0.6	-32.2	1.1	-20.5	3.4	-21.5	1.4	-18.3	2.3	-22.7	2.2
KABSLX	-25.7	1.3	-30.7	1.9	-19.9	3.7	-22.3	1.6	-20.4	3.7	-24.4	2.0
TDKEM	-14.4	1.4	-13.4	1.3	-17.4	0.4	-16.5	1.6	-16.5	0.4	0.0	0.0

Zeta potential of most of the minerals after three days of immersion in complete cell culture media is close to -20 mV regardless of the initial zeta potential value. This value is similar to the zeta potential measured in the literature for the native BSA at the cell culture pH conditions [50]. Following the results from the FTIR, the changes to the zeta potential are a result from the adsorption of the proteins from the serum onto the minerals. In cases where the adsorption bands were not observed, such as the unmodified calcium carbonates, it might be that the interacting layer was too thin to be recognised by the FTIR method utilised. Additionally, weak adsorptions may not withstand the washing and drying process of the sample preparation.

Only two minerals had positive zeta potentials initially: CCOBIND and CCOMYA. The zeta potential of CCOBIND changed to approx. -1 mV and -21 mV in the presence of serum-free cell culture media and complete DMEM, respectively and regardless of the time of immersion. In contrast, the zeta potential of CCOMYA changed significantly only in the presence of serum. This might affect the interaction with the fibroblasts since the minerals are first suspended in serum-free media, and they only enter into contact with serum upon addition to the cells. Therefore, CCOMYA could potentially be the only mineral with a positive zeta potential when entering the cellular environment.

Other remarkable samples in terms of the zeta potential were the calcium sulphates. The $CaSO_4.2H_2O$ samples (CS2H2O, and CSANAL) did not exhibit changes in the zeta potential. There are two possible reasons for this, related to the dissolution of the samples. The rate of dissolution of the minerals could compete against the rate of adsorption limiting the surface area, and active sites for adsorption, available to the molecules in the cell culture media. Similarly, any adsorption of the proteins onto the surface may be removed due to dissolution during the sample preparation. Lastly, the calcium sulphate hemihydrate is a difficult sample to analyse. Calcium sulphate hemihydrates start immediately a transformation to calcium sulphate dihydrate upon contact with water. It starts with the dissolution of the hemihydrate to saturate the solution with Ca^{2+} and SO_4^{2-} ions, followed by the nucleation and crystal growth of the dihydrate form. A major factor affecting this process is the presence of molecules that may act as accelerators or retarders [51]. In contrast to water, the cell culture media is a complex mixture that contains inorganic salts, amino acids, carbohydrates, proteins, peptides, fatty acids, lipids, vitamins, hormones, growth factors, protease inhibitors, minerals, trace elements, and antibiotics [52]. Therefore, it is difficult to determine how the accelerators and/or retardants are affecting the dissolution and transformation of the hemihydrate. However, the FTIR spectra together with the zeta potential suggest a high adsorption of molecules onto the CSINDUS surface that inhibits the formation of $CaSO_4.2H_2O$.

In general, the initial zeta potential of the minerals may not play actively a role on cell behaviour since it is largely controlled by the protein adsorption. Instead, it can be a passive interaction that potentially modifies the structural behaviour of the proteins adsorbed into the mineral surfaces, and therefore affect what the fibroblasts sense in their environment.

Interaction between HDF cells and the mineral particles

The first assessment of interaction between the mineral particles and the human dermal fibroblasts involved the MTT assay, LDH assay, and the percentage of coverage of cells obtained from the live cell imaging (protocol in Appendix A). The data is summarised in Figure 3, showing the value for each sample relative to the control sample. Appendix A includes original data (Tables A.2-4) and representative images (Figure A.19-23) for each mineral-cell interaction.

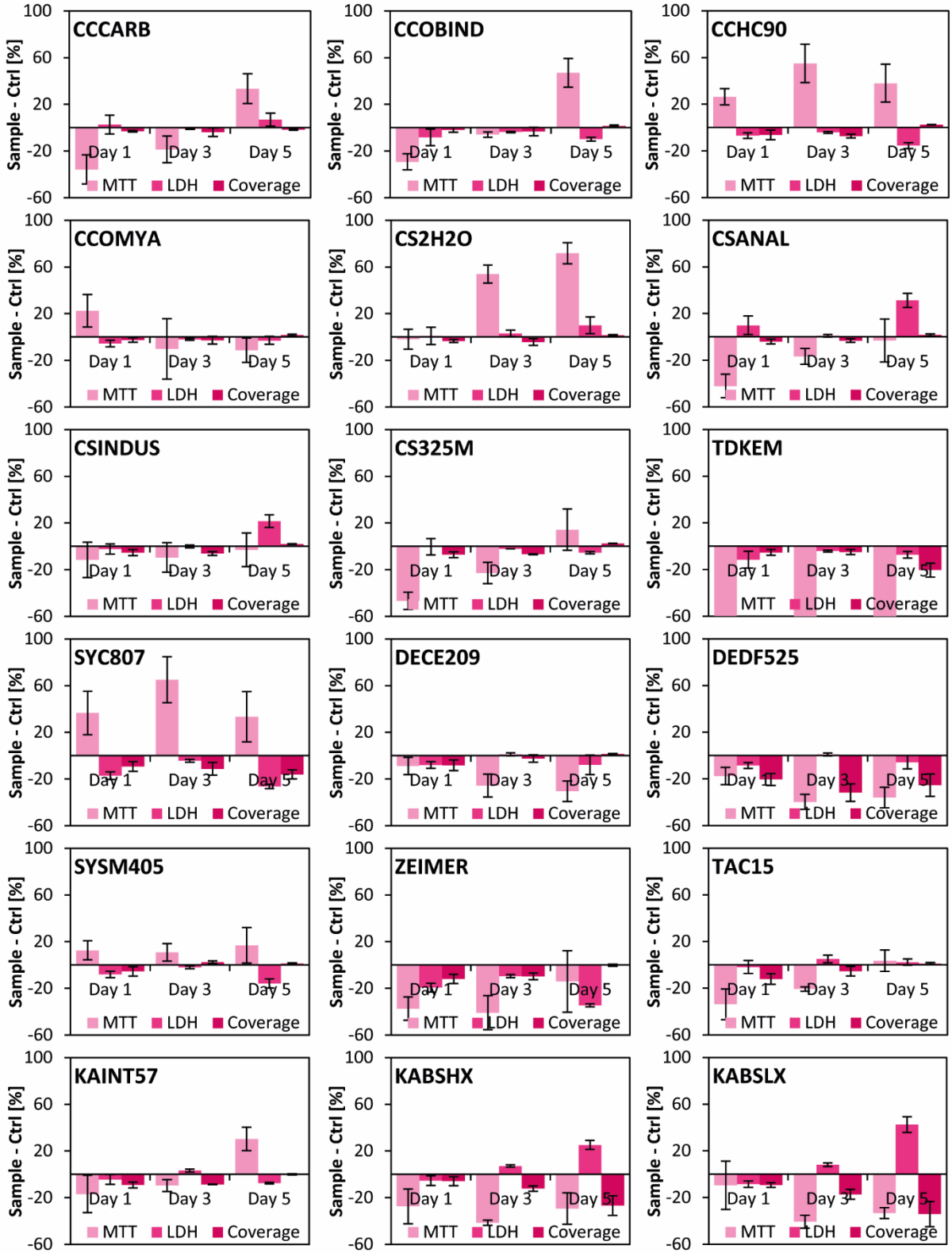

Figure 3. Biological assessment of minerals through colorimetric assays expressed as the difference between the mineral-treated sample (Sample), and the untreated control (Ctrl). The percentages for each study refer to: viability (MTT assay), cytotoxicity (LDH assay), and area of coverage (Calcein AM). Error bars: SEM.

The assessment included observations from the images such as the apparent proliferation, cell shape, localisation of the cells compared to the particles, and pattern formation. Based on the

observed/quantified biological interaction, Figure 4 proposes a classification of the minerals according to their time-dependent cellular response.

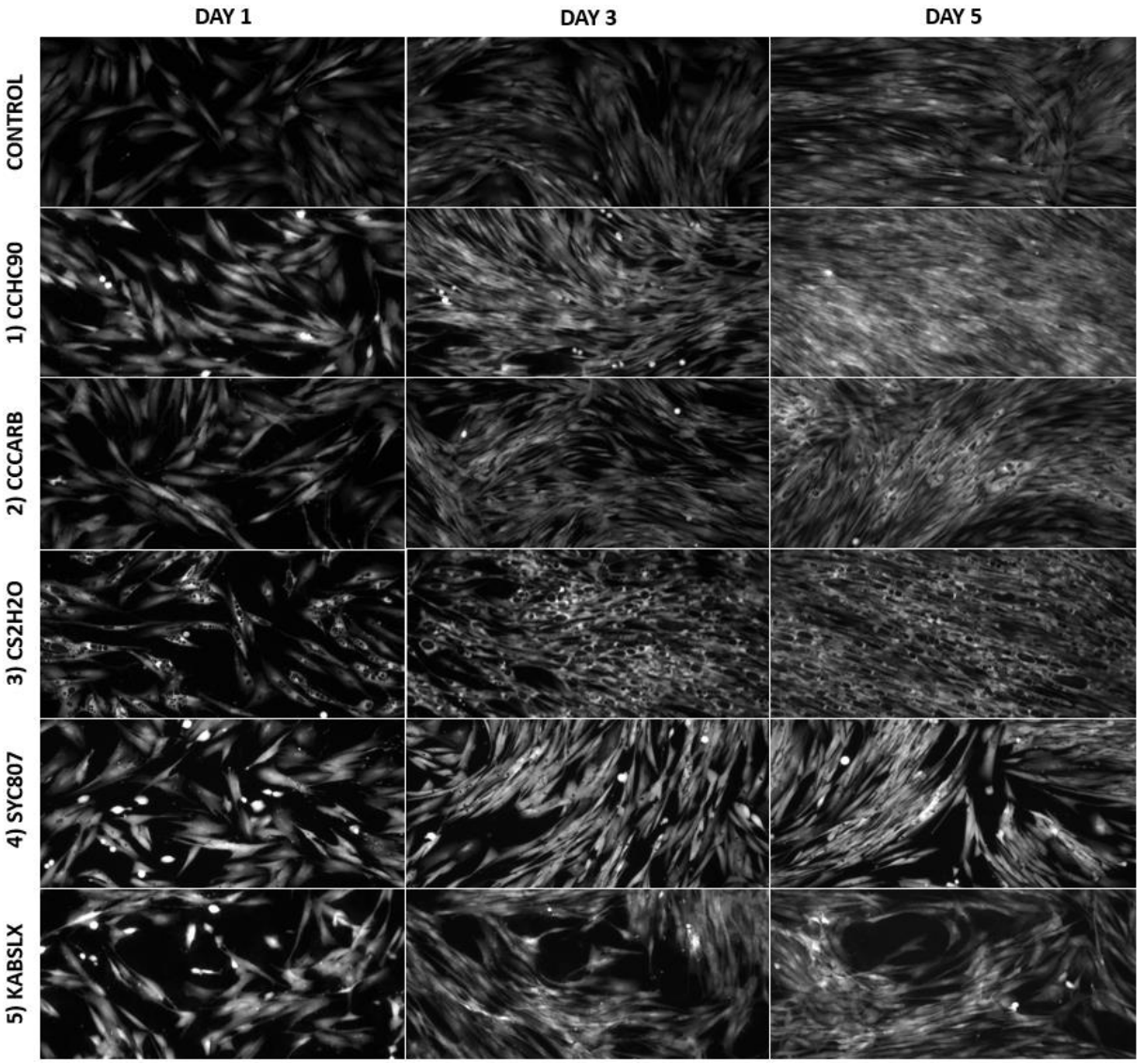

GROUP 1 Enhanced proliferation with fast recovery	GROUP 2 Enhanced proliferation with slow recovery	GROUP 3 Enhanced proliferation with vacuolisation	GROUP 4 Growth inhibition	GROUP 5 Cytotoxicity
CCHC90 CCOBIND CCOMYA TAC15	DECE209 SYSM405 CCCARB ZEIMER KAINT57	CSANAL CS2H2O CSINDUS CS325M	TDKEM SYC807 DEDF525	KABSHX KABSLX

LONG-TERM USE — SHORT-TERM USE

Figure 4. Suggested classification of minerals based on the investigated biological interactions, and representative cell culture images of one mineral per group after one, three, and five days of interaction.

Group 1 represents the minerals that led to enhanced proliferation with fast recovery. Fast recovery means that despite the initial slight decrease in proliferation, by day three the cells were comparable to

the control samples and by day five they were over-proliferating. Group 2 includes minerals that enhance proliferation of cells only after five days possibly due to an extended period of adaptation from the cells to the minerals. In Group 1 and 2, the increase in proliferation was preceded by decrease in cell size. Smaller/thinner, elongated cells meant that a larger amount of cells could fit in the same available area for growth.

Group 3 contained minerals that enhance cell proliferation, yet they induce a significant morphological change in the fibroblasts in the form of cytoplasmic vacuoles. This group is comprised exclusively of the calcium sulphate samples, suggesting that calcium ions play a key role in the induced cell fate. Group 4 includes minerals for which the cells did not recover, and instead showed growth inhibition in long term. DEDF525 is a particular sample that has similar characteristics to DECE209 yet the response is opposite. It is possible that the difference in shape, porosity and impurities detected in their FTIR spectra play a role. Furthermore, this group contained minerals of nanoscale (TDKEMIR, and SYC807) where the interaction with the cells is partially defined by the internalisation of the particles. At last, minerals in Group 5 induced cytotoxic response in the fibroblasts. In comparison to KAINT57 (not detrimental to the cells), both KABSHX and KABSLX have a very platy particle shape. The increased shape factor reduces the amount of exposed aluminol and silanol groups at the particle edges, which potentially modifies the interaction with cells. In addition, the edge "height" (particle thickness) of KABSHX and KABSLX is less than 50 nm, potentially allowing local partial internalisation by the cells.

Live cell imaging videos showed mineral affinity to the cells, as the particles moved with the cells and led to cell agglomerations. Larger particles, such as CCCARB, ZEIMER, and KAINT57, affected pattern formation of the HDFs as cells concentrated around the minerals. This is possibly caused by the larger size of the particles acting as physical obstacles, and the affinity of the cells to the minerals. The videos also show that, in time, some of the mineral particles aggregate. In this study, particles are not stabilised with additives. Particles with an absolute value of zeta potential smaller than approx. 30 mV are unstable and will tend to aggregate despite the initial mechanical dispersion. The aggregation is also facilitated by the affinity and movement of the cells, and the Brownian motion of smaller particles.

The evaluation of the time-dependent response of HDFs to the minerals provides fundamental insight into the mineral-cell interactions. Minerals included in Group 1 and 2, for example, are suitable to enhance proliferation for extended periods of time. Groups 4 is best for short time exposure to the cells due to long-term growth inhibition, while Group 5 presents long-term toxicity. Further studies could identify whether cells can recover from exposure to minerals in Group 4 and 5 or the behaviours are irreversible. Then, alternative applications can be considered for these minerals. The use of particles in a biological environment is challenging due to incomplete understanding on how their physicochemical properties can influence cell behaviour or interfere with current experimental methods [53]. Therefore, extrapolation from *in vitro* to *in vivo* studies is not suggested before a thorough characterisation and toxicological assessment has been carried. This study encourages future *in vitro* research on the mineral interactions with cells to continue expanding the available knowledge and minimise potential safety concerns.

Stress and apoptotic response to the minerals

Cells also react to changes in their environment by activating stress responses. The heat shock response (HSR) protects cells from proteotoxic stresses by activating heat shock factors (HSFs) that promote the transcription of heat shock proteins (Hsps) [54]. Hsps are molecular chaperones that envelope and stabilize proteins, allowing them to fold and function correctly. They are thus used as markers for

proteotoxic stresses when evaluating the biocompatibility of materials or treatments of cells [55,56]. Another important marker to consider is Poly [ADP-ribose] polymerase 1 (PARP1), a nuclear protein involved in DNA repair that is cleaved into 89 kDa and 24 kDa fragments in the event of apoptosis, a form of cell death [57]. Therefore, to understand the fibroblasts' response to the minerals, the protein levels of the HSR markers Hsp90, Hsp70, Hsp27, and HSF1, and of the apoptotic marker PARP1, were analysed by western blotting (Figure 5A-F).

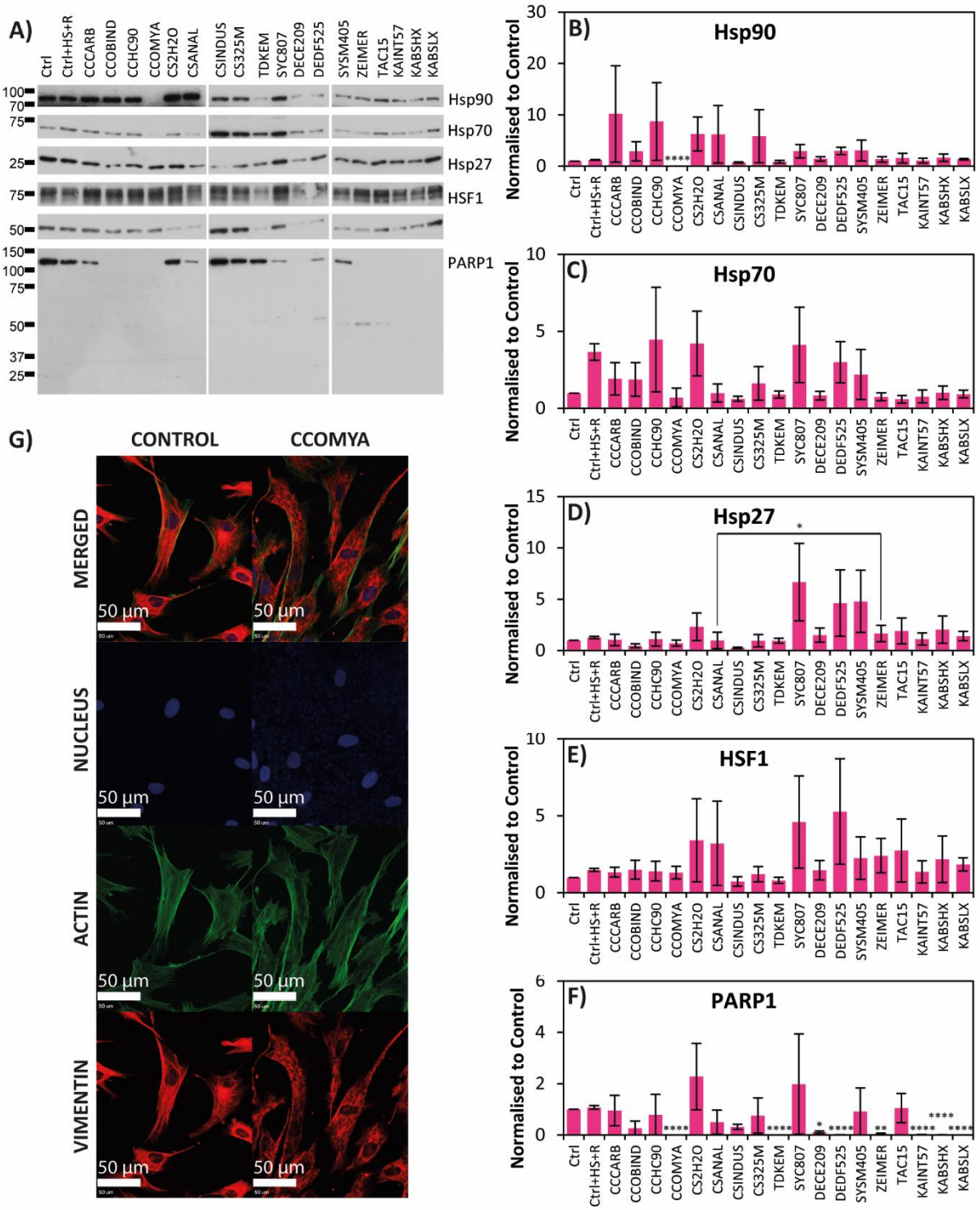

Figure 5. **A-F)** Analysis of cell stress markers of treated cells. Cells were lysed and analysed by western blotting with antibodies against Hsp90, Hsp70, Hsp27, HSF1, and PARP1. The blots were quantified

using ImageJ by normalizing the protein levels to the loading control alpha tubulin. Statistical analyses were performed with GraphPad Prism 7 using ANOVA, followed by Tukey's test. Results from control (Ctrl) were compared to mineral samples (p: ns>0.05, * ⩽0.05, **⩽0.01, ***⩽0.001, ****⩽0.0001, error bars: SEM, B-F). Other significant comparisons are shown with a line connecting both mineral samples. **G)** Spinning disk imaging of untreated (CONTROL) and cells treated with CCOMYA, and stained for nucleus, actin, and vimentin.

Hsp90 levels changed significantly only for CCOMYA, where the levels were depleted (Figure 5A&B). Hsp90 has been found to have strong binding capabilities to amorphous calcium phosphate (ACP) and to hydroxyapatite, forming so called protein-mineral complexes (PMC) [58]. FTIR spectra of CCOMYA revealed peaks similar to those of phosphate groups in addition to the ones corresponding to calcium carbonate. Therefore, a similar process involving the phosphate groups of CCOMYA may be taking place since the interaction is exclusive to the Hsp90 protein. Further studies are needed to verify the formation of the PMC, and whether it takes place inside the cells due to the internalisation of the minerals or extracellularly, during the lysis of the cells. However, changes observed to the vimentin structure of the cell (Figure 6G) show a response from the cell to CCOMYA already during treatment that could be related to the PMC. Given the importance of Hsp90 in cancer [58-60], the potential affinity to Hsp90 opens new possible applications of study for CCOMYA.

No PARP1 apoptotic cleavage was detected among the samples, but several minerals showed significant downregulation and depletion of full-length PARP1 (Figure 5A&F). Most of them were silica-containing minerals (DECE209, DEDF525, ZEIMER, KAINT57, KABSHX, and KABSLX). Silica reduces mRNA levels of PARP1, but the exact mechanism is unknown [61]. As for the rest of the Hsps, fluctuations in Hsp27, Hsp70 and HSF1 levels were not significantly changed by most of the minerals (Figure 5C-E). The lack of significant changes indicates that the cells were not proteotoxically stressed nor apoptosis was induced by the mineral samples. However, some minerals had large variations in the response, which means that the results from those samples are not conclusive, and require further attention in future studies.

Vacuolisation of human dermal fibroblasts

Calcium sulphates induced a morphological change to the HDFs. Calcein AM staining revealed what appears to be cytoplasmic vacuolisation of the cells when interacting with the calcium sulphates. The vacuolisation was extensively visible even with the light microscope. It started approximately two hours after the addition of the minerals and remained present throughout the five days of interaction. The 'vacuoles' were present close to the cell nucleus and had varying sizes and shapes sometimes occupying most of the cellular structure, yet not inducing cell death.

The observed cytoplasmic vacuoles shared similarities to lipid droplets. However, preliminary studies (not shown) included perilipin and Oil Red O staining and neither showed a response from the vacuoles. Instead, the spinning disk images (Figure 6) suggest that the vacuoles were inside the cells and enclosed by vimentin filaments. Recommended future studies include additional immunofluorescence staining and TEM imaging of the vacuoles in order to verify the location and composition of the vacuoles.

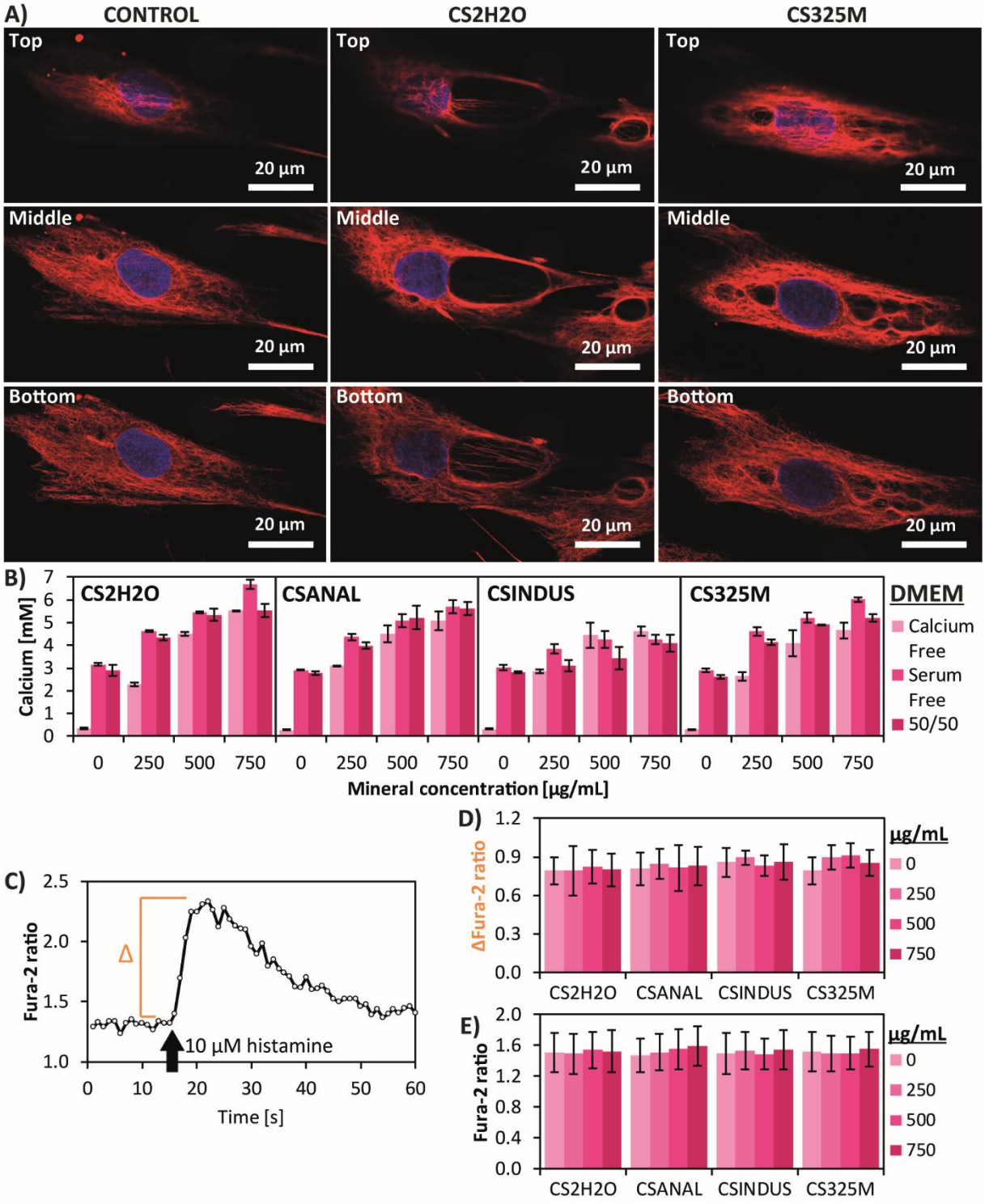

Figure 6. **A)** Spinning disk images of cells untreated (CONTROL) and treated with CS2H2O, and CS325M (150 µg/mL). **B)** Extracellular calcium ion concentration after one day of calcium sulphate treatments of different concentrations in calcium free, serum free, and 50/50 serum-free/complete DMEM. **C-D)** Intracellular calcium levels in HDFs were analysed with the fluorescent calcium indicator Fura-2 AM after on day of calcium sulphate treatments. Figure 6C shows a representative experiment where the basal calcium levels were recorded for 15 seconds where after the cells were stimulated with 10 µM histamine when indicated by the arrow. Figure 6D shows the analysis of the change in Fura-2 ratio after histamine treatment (basal value subtracted from the maximal histamine stimulated value). Figure 6E shows the analysis of the basal calcium values indicated by the Fura-2 ratio.

The mineral SYC807 also showed vacuoles in the Calcein AM staining. However, the vacuoles were small and not concentrated towards the nucleus, while the cells were largely elongated compared to the spindle-shape morphology of the control cells. For this mineral, the cell growth was inhibited, suggesting that the mechanism behind the morphological change was different. According to literature, small silica nanoparticles (approx. 10 nm) decrease cell viability of HDFs and are rapidly internalised by the cells in endocytic vesicles while inducing elongation of the HDFs and cell membrane damage [62,63]. Similarly, polymeric silicic acid imparts structural changes to primary lung fibroblasts, including cytoplasmic vacuoles and lipoids, which are detrimental to the cells [64]. While SYC807 does not damage the cell membrane, possibly due to the aggregation of the nanoparticles prior to the uptake, the increased metabolic activity and the possible arrest in cell growth shows that the cells are responding to the stress provided by the mineral.

The results herein show that the calcium sulphates present unreported significant and extensive morphological changes in cells while enhancing their proliferation. The biological assessment indicated signs of cell membrane damage after five days of interaction for calcium sulphates, except for CS325M, the mineral with the largest size within the group. Therefore, the harmful response can be a result of the particular size or shape of the minerals. In general, cytoplasmic vacuolisation plays an important role in the adaptation process of cells, and it is usually related to cell death [65,66]. These minerals could provide further understanding to cytoplasmic vacuolisation.

Extracellular and intracellular calcium studies

Figure 6B shows the extracellular calcium concentration after one day of calcium sulphate treatment with three concentrations, and considering three cell culture media environments: calcium free, serum-free and the 50/50 serum-free/complete DMEM. The addition of calcium sulphate particles to the cellular environment resulted in a significant increase of calcium ion concentration regardless of the initial presence of calcium or serum in the media. The higher the concentration of particles, the higher the release of calcium ions. However, the presence of serum (50/50) led to a decrease in the calcium concentration when compared to the serum-free environment. Thus, the serum components may either reduce the solubility of the calcium sulphates or bind the free ions once they are in solution. The lowest release of calcium ions was observed for CSINDUS, which is the calcium sulphate hemihydrate, possibly due to the interaction with the components of the cell culture media. The significant increase of extracellular calcium ion concentration indicate that the calcium sulphates studied could be used as a calcium source to cells, and that these minerals are of interest for studies with cell lines that are sensible to changes to the extracellular calcium levels.

Calcium ions are extremely important for the cellular signalling and are involved multiple processes within and between the cells [67]. These processes include cell proliferation, migration, cellular respiration as well as regulation of programmed cell death. Consequently, the intracellular calcium concentration is tightly regulated. A significant increase in the extracellular calcium ion concentration such as the one generated by the calcium sulphates can potentially induce changes in the intracellular calcium levels. Disturbances in intracellular calcium handling might lead to detrimental effects, such as the initiation of programmed cell death. Therefore, we assessed whether the calcium-releasing minerals CS2H2O, CSANAL, CSINDUS, and CS325M affect the basal cytoplasmic calcium levels or the cytoplasmic calcium levels upon an agonist stimulation. We found that both the agonist-induced as well as the basal calcium levels were unchanged after treating the cells with the minerals (Figure 6C-E). This indicates that the minerals do not significantly or detrimentally alter the calcium handling of the HDFs.

CONCLUSION

In this article, human dermal fibroblasts were treated with different samples of calcium carbonates, calcium sulphates, silica, silicates, and titanium dioxide. Minerals were characterised, and their influence on the fibroblasts behaviour was assessed and compared to their properties. Results show that a shared initial cellular response to the minerals is followed by enhanced proliferation, growth inhibition, or cell damage. Therefore, minerals were grouped according to the cellular response as a function of time, providing fundamental insight into the interactions. Mineral properties such as size, solubility, and chemical composition had direct effects on the cells. Larger particles acted as physical obstacles to the cells, promoting agglomeration of cells around the minerals. Calcium sulphates induced a significant change in the fibroblast morphology similar to cytoplasmic vacuolisation. It is suggested that the morphological features are related to the significant increase in extracellular calcium ion levels, yet no changes to the intracellular calcium were observed. Additionally, a modified calcium carbonate downregulated both α- and β-Hsp90, and PARP1 in fibroblasts, possibly through the formation of protein-mineral complexes. The zeta potential of the minerals is dominated by the protein adsorption from the cell culture media. Thus, surface-mediated conformational changes to the adsorbed proteins may affect cellular processes that depend on feedback from the surface protein layer.

In order to verify the changes to cell behaviour, further studies would be needed. For this article, the observations and experiments were enough to elucidate the general biological interaction between the minerals and the HDFs. The potential presence of dispersants in some of the minerals, such as kaolin, might add uncertainty to this study. Therefore, future studies will investigate the influence of dispersants and other mineral additives on cell behaviour.

ACKNOWLEDGMENTS

Doctoral Network of Material Sciences from Åbo Akademi University for the financial support. The FunMat Consortia, more specifically the Laboratory of Prof. John Eriksson for providing the facilities for the cellular studies. All the imaging was possible thanks to the Cell Imaging Core at the Turku Centre for Biotechnology in Turku, Finland.

REFERENCES

1. Stevens MM, George JH. Exploring and Engineering the Cell Surface Interface. Science 2005;310:1135.
2. Guilak F, Cohen DM, Estes BT, Gimble JM, Liedtke W, Chen CS. Control of stem cell fate by physical interactions with the extracellular matrix. Cell Stem Cell 2009;5:17-26.
3. Perkins TJ, Swain PS. Strategies for cellular decision‐making. Mol Syst Biol 2009;5.
4. Gane PAC. Mineral pigments for paper : Structure, function and development potential (Part I). Wochenblatt für Papierfabrikation 2015;129:110-116.
5. Murray HH, Batruk SJ, Boland MP, Brooks AM, Hagemeyer RW, Koenig JJ, et al. Paper coating pigments. The United States of America: Technical Association of the Pulp and Paper Industry, 1966.
6. Hughes E, Yanni T, Jamshidi P, Grover LM. Inorganic cements for biomedical application: calcium phosphate, calcium sulphate and calcium silicate. Advances in Applied Ceramics 2015;114:65-76.
7. Mazor Z, Mamidwar S, Ricci JL, Tovar NM. Bone repair in periodontal defect using a composite of allograft and calcium sulfate (DentoGen) and a calcium sulfate barrier. J Oral Implantol 2011;37:287-292.
8. Xiaohong Wang and Maximilian Ackermann and Shunfeng Wang and Emad Tolba and Meik Neufurth and Qingling Feng and Heinz C Schröder and Werner, E G M. Amorphous

polyphosphate/amorphous calcium carbonate implant material with enhanced bone healing efficacy in a critical-size defect in rats. Biomedical Materials 2016;11:035005.
9. Dewi AH, Ana ID, Jansen J. Preparation of a calcium carbonate-based bone substitute with cinnamaldehyde crosslinking agent with potential anti-inflammatory properties. Journal of Biomedical Materials Research Part A 2017;105:1055-1062.
10. Shen Y, Yang S, Liu J, Xu H, Shi Z, Lin Z, et al. Engineering scaffolds integrated with calcium sulfate and oyster shell for enhanced bone tissue regeneration. ACS Appl Mater Interfaces 2014;6:12177-12188.
11. Thomas MV, Puleo DA. Calcium sulfate: Properties and clinical applications. J Biomed Mater Res 2009;88B:597-610.
12. Clapham DE. Calcium signaling. Cell 2007;131:1047-1058.
13. Fujiwara M, Shiokawa K, Morigaki K, Zhu Y, Nakahara Y. Calcium carbonate microcapsules encapsulating biomacromolecules. Chemical Engineering Journal 2008;137:14-22.
14. Zhao D, Wang CQ, Zhuo RX, Cheng SX. Modification of nanostructured calcium carbonate for efficient gene delivery. Colloids Surf B Biointerfaces 2014;118:111-116.
15. Maleki Dizaj S, Barzegar-Jalali M, Zarrintan MH, Adibkia K, Lotfipour F. Calcium carbonate nanoparticles as cancer drug delivery system. Expert Opin Drug Deliv 2015;12:1649-1660.
16. Lu C, Hung Y, Hsiao J, Yao M, Chung T, Lin Y, et al. Bifunctional Magnetic Silica Nanoparticles for Highly Efficient Human Stem Cell Labeling. Nano Lett 2007;7:149-154.
17. Hsiao J, Tsai C, Chung T, Hung Y, Yao M, Liu H, et al. Mesoporous Silica Nanoparticles as a Delivery System of Gadolinium for Effective Human Stem Cell Tracking. Small 2008;4:1445-1452.
18. Lipski AM, Pino CJ, Haselton FR, Chen I-, Shastri VP. The effect of silica nanoparticle-modified surfaces on cell morphology, cytoskeletal organization and function. Biomaterials 2008;29:3836-3846.
19. Lu F, Wu S, Hung Y, Mou C. Size Effect on Cell Uptake in Well-Suspended, Uniform Mesoporous Silica Nanoparticles. Small 2009;5:1408-1413.
20. Huang X, Li L, Liu T, Hao N, Liu H, Chen D, et al. The Shape Effect of Mesoporous Silica Nanoparticles on Biodistribution, Clearance, and Biocompatibility in Vivo. ACS Nano 2011;5:5390-5399.
21. Bariana M, Aw MS, Losic D. Tailoring morphological and interfacial properties of diatom silica microparticles for drug delivery applications. Advanced Powder Technology 2013;24:757-763.
22. Delalat B, Sheppard VC, Rasi Ghaemi S, Rao S, Prestidge CA, McPhee G, et al. Targeted drug delivery using genetically engineered diatom biosilica. 2015;6:8791.
23. Pourshahrestani S, Zeimaran E, Djordjevic I, Kadri NA, Towler MR. Inorganic hemostats: The state-of-the-art and recent advances. Mater Sci Eng C Mater Biol Appl 2016;58:1255-1268.
24. Davies R, Griffiths DM, Johnson NF, Preece AW, Livingston DC. The cytotoxicity of kaolin towards macrophages in vitro. Br J Exp Pathol 1984;65:453-466.
25. Wallace WE, Vallyathan V, Keane MJ, Robinson V. In vitro biologic toxicity of native and surface‐modified silica and kaolin. J Toxicol Environ Health 1985;16:415-424.
26. Michel C, Herzog S, de Capitani C, Burkhardt-Holm P, Pietsch C. Natural mineral particles are cytotoxic to rainbow trout gill epithelial cells in vitro. PLoS One 2014;9:e100856.
27. Awad ME, López-Galindo A, Setti M, El-Rahmany MM, Iborra CV. Kaolinite in pharmaceutics and biomedicine. International Journal of Pharmaceutics 2017;533:34-48.
28. Zhang Y, Long M, Huang P, Yang H, Chang S, Hu Y, et al. Intercalated 2D nanoclay for emerging drug delivery in cancer therapy. Nano Research 2017;10:2633-2643.
29. Longo DL, Young RC. COSMETIC TALC AND OVARIAN CANCER. The Lancet 1979;314:349-351.
30. Nasreen N, Hartman DL, Mohammed KA, Antony VB. Talc-induced expression of C-C and C-X-C chemokines and intercellular adhesion molecule-1 in mesothelial cells. Am J Respir Crit Care Med 1998;158:971-978.
31. Nasreen N, Mohammed KA, Dowling PA, Ward MJ, Galffy G, Antony VB. Talc induces apoptosis in human malignant mesothelioma cells in vitro. Am J Respir Crit Care Med 2000;161:595-600.
32. Nasreen N, Mohammed KA, Brown S, Su Y, Sriram PS, Moudgil B, et al. Talc mediates angiostasis in malignant pleural effusions via endostatin induction. Eur Respir J 2007;29:761-769.

33. Buz'Zard AR, Lau BHS. Pycnogenol® reduces talc-induced neoplastic transformation in human ovarian cell cultures. Phytotherapy Research 2007;21:579-586.
34. Wentzensen N, Wacholder S. Talc use and ovarian cancer: epidemiology between a rock and a hard place. J Natl Cancer Inst 2014;106:10.1093/jnci/dju260.
35. ERSOY B, DIKMEN S, YILDIZ A, GREN R, ELITOK m. Mineralogical and physicochemical properties of talc from Emirdag, Afyonkarahisar, Turkey. Turkish Journal of Earth Sciences 2013;22:632-644.
36. Arsoy Z, Ersoy B, Evcin A, İçduygu MG. Influence of dry grinding on physicochemical and surface properties of talc. Physicochemical Problems of Mineral Processing 2016;53:288-306.
37. Oliveira WF, Arruda IRS, Silva GMM, Machado G, Coelho, Luana C B B, Correia MTS. Functionalization of titanium dioxide nanotubes with biomolecules for biomedical applications. Materials Science and Engineering: C 2017;81:597-606.
38. Juvonen H, Maattanen A, Lauren P, Ihalainen P, Urtti A, Yliperttula M, et al. Biocompatibility of printed paper-based arrays for 2-D cell cultures. Acta Biomater 2013;9:6704-6710.
39. Ng K, Gao B, Yong KW, Li Y, Shi M, Zhao X, et al. Paper-based cell culture platform and its emerging biomedical applications. Materials Today 2017;20:32-44.
40. Kenney RM, Lloyd CC, Whitman NA, Lockett MR. 3D cellular invasion platforms: how do paper-based cultures stack up? Chem Commun 2017;53:7194-7210.
41. Coulomb B, Lebreton C, Dubertret L. Influence of human dermal fibroblasts on epidermalization. J Invest Dermatol 1989;92:122-125.
42. Schindelin J, Rueden CT, Hiner MC, Eliceiri KW. The ImageJ ecosystem: An open platform for biomedical image analysis. Mol Reprod Dev 2015;82:518-529.
43. Schindelin J, Arganda-Carreras I, Frise E, Kaynig V, Longair M, Pietzsch T, et al. Fiji: an open-source platform for biological-image analysis. Nat Methods 2012;9:676-682.
44. Francis GL. Albumin and mammalian cell culture: implications for biotechnology applications. Cytotechnology 2010;62:1-16.
45. Grdadolnik J, Maréchal Y. Bovine serum albumin observed by infrared spectrometry. I. Methodology, structural investigation, and water uptake. Biopolymers 2001;62:40-53.
46. Servagent-Noinville S, Revault M, Quiquampoix H, Baron M. Conformational Changes of Bovine Serum Albumin Induced by Adsorption on Different Clay Surfaces: FTIR Analysis. J Colloid Interface Sci 2000;221:273-283.
47. Socrates G. Infrared and raman characteristic group frequencies. 3. ed., reprinted as paperback ed. Chichester [u.a.]: Wiley, 2006.
48. Zeng H, Chittur KK, Lacefield WR. Analysis of bovine serum albumin adsorption on calcium phosphate and titanium surfaces. Biomaterials 1999;20:377-384.
49. Roach P, Farrar D, Perry CC. Interpretation of Protein Adsorption: Surface-Induced Conformational Changes. J Am Chem Soc 2005;127:8168-8173.
50. Vilker VL, Colton CK, Smith KA. The osmotic pressure of concentrated protein solutions: Effect of concentration and ph in saline solutions of bovine serum albumin. Journal of Colloid and Interface Science 1981;79:548-566.
51. Singh NB, Middendorf B. Calcium sulphate hemihydrate hydration leading to gypsum crystallization. Progress in Crystal Growth and Characterization of Materials 2007;53:57-77.
52. Arora M. Cell Culture Media: A Review. Materials and Methods 2013;3:175.
53. Kroll A, Pillukat MH, Hahn D, Schnekenburger J. Current in vitro methods in nanoparticle risk assessment: Limitations and challenges. European Journal of Pharmaceutics and Biopharmaceutics 2009;72:370-377.
54. Marek A. Budzyński and Lea Sistonen*. Versatile Functions of Heat Shock Factors: It is Not All About Stress. Current Immunology Reviews 2017;13:4-18.
55. OSHIMA H, HATAYAMA T, NAKAMURA M. A possibility for new evaluating method of cytotoxicity by using heat shock protein assay. J Mater Sci Mater Med 1997;8:143-147.
56. Joly A-, Wettstein G, Mignot G, Ghiringhelli F, Garrido C. Dual Role of Heat Shock Proteins as Regulators of Apoptosis and Innate Immunity. J Innate Immun 2010;2:238-247.
57. Chaitanya GV, Alexander JS, Babu PP. PARP-1 cleavage fragments: signatures of cell-death proteases in neurodegeneration. Cell Communication and Signaling : CCS 2010;8:31.

58. Lianos GD, Alexiou GA, Mangano A, Mangano A, Rausei S, Boni L, et al. The role of heat shock proteins in cancer. Cancer Letters 2015;360:114-118.
59. Hong DS, Banerji U, Tavana B, George GC, Aaron J, Kurzrock R. Targeting the molecular chaperone heat shock protein 90 (HSP90): Lessons learned and future directions. Cancer Treatment Reviews 2013;39:375-387.
60. Jhaveri K, Ochiana SO, Dunphy MPS, Gerecitano JF, Corben AD, Peter RI, et al. Heat shock protein 90 inhibitors in the treatment of cancer: current status and future directions. Expert Opin Investig Drugs 2014;23:611-628.
61. Gao A, Song S, Wang D, Peng W, Tian L. Effect of silicon dioxide on expression of poly (ADP-Ribose) polymerase mRNA and protein. Cell Biol Int 2009;33:749-754.
62. Quignard S, Mosser G, Boissière M, Coradin T. Long-term fate of silica nanoparticles interacting with human dermal fibroblasts. Biomaterials 2012;33:4431-4442.
63. Zhang Y, Hu L, Yu D, Gao C. Influence of silica particle internalization on adhesion and migration of human dermal fibroblasts. Biomaterials 2010;31:8465-8474.
64. Linthicum DS. Ultrastructural effects of silicic acid on primary lung fibroblasts in tissue culture. Tissue and Cell 2001;33:514-523.
65. Henics T, Wheatley DN. Cytoplasmic vacuolation, adaptation and cell death: A view on new perspectives and features. Biology of the Cell 1999;91:485-498.
66. Shubin AV, Demidyuk IV, Komissarov AA, Rafieva LM, Kostrov SV. Cytoplasmic vacuolization in cell death and survival. Oncotarget 2016;7:55863-55889.
67. Berridge MJ, Lipp P, Bootman MD. The versatility and universality of calcium signalling. Nat Rev Mol Cell Biol 2000;1:11-21.